PCCP

PAPER

View Article Online
View Journal | View Issue

Cite this: Phys. Chem. Chem. Phys., 2025, 27, 22004

Core-level binding energies describe electrostatic potentials at nuclei for ionic liquids

Frances K. Towers Tompkins,[a] Ekaterina Gousseva,[a] Roger A. Bennett,[a]
Ricardo Grau-Crespo[ab] and Kevin R. J. Lovelock*[a]

Received 24th June 2025,
Accepted 23rd September 2025

DOI: 10.1039/d5cp02411k

rsc.li/pccp

Electrostatic interactions in ionic liquids (ILs) dictate many of their physical properties and hence underpin a plethora of potential applications. It is vital to develop both experimental and theoretical electronic descriptors for ILs, to drive deeper understanding of the interactions that may be tuned for applications. A possible descriptor for ILs is the readily measurable core-level binding energy from experimental core-level X-ray photoelectron spectroscopy (XPS), E_B(core). To establish that differences in E_B(core) capture the differences in electrostatic potential at nuclei, V_n, we use a computational approach based on *ab initio* molecular dynamics (AIMD). We demonstrate clear quantitative (linear) correlations between experimental E_B(core) and calculated V_n for carbon, nitrogen, sulfur, oxygen and fluorine for both cations and anions. Our work shows that E_B(core) are chemically interpretable descriptors of electrostatic interactions in ILs. This has implications for the ability to predict, out of the vast number of ILs that can form from the array of available cations and anions, the best IL compositions for target applications. We also discuss how this work could open up new areas of enquiry, and the potential usefulness of V_n to characterise interactions of ILs with surfaces and interfaces.

1. Introduction

Electrostatic interactions in ionic liquids (ILs) – liquids composed solely of ions – dominate both ion–ion and ion–neutral molecule interactions. These interactions underpin the physical and chemical properties of the liquids, and hence a plethora of potential applications of ILs.[1–7] Many models of ILs do not consider electrostatic interactions at atomic level, including in domain analysis (example groups include charged groups, hydrocarbons, fluorous)[8] and coarse-grain models (*e.g.* hard-sphere cations and anions).[9,10] However, for interactions of ILs with solutes, particularly metal cations of interest in battery electrolytes such as Li^+, *e.g.* Li^+–O, Li^+–N and Li^+–F interactions for Li^+ dissolved in an $[NTf_2]^-$-based IL ($[NTf_2]^-$ = bis[(trifluoromethane)sulfonyl]imide), local electrostatic interactions will matter. Therefore, it is vital to develop both experimental and calculated local electronic structure descriptors to aid the selection of the best IL for a given target application, from the thousands of IL composition possibilities.[11]

Two very commonly used local electronic structure descriptors for molecular systems, oxidation state and atomic charge, are only of limited use for understanding and predicting electrostatic interactions in ILs. Oxidation states are not helpful for ILs given their inability to reflect differences in chemical bonding and valence electron location. For example, nitrogen has a formal oxidation state of −3 in most IL ions, including both common cations (*e.g.* $[C_8C_1Im]^+$ = 1-*n*-octyl-3-methylimidazolium) and common anions (*e.g.* $[NTf_2]^-$ and $[SCN]^-$ = thiocyanate), but is +3 in $[NO_3]^-$ = nitrate; chemical intuition strongly suggests that the nitrogen atoms in $[C_8C_1Im]^+$ and $[NTf_2]^-$ are not electronically identical. Atomic charge (at times known as partial charge), which has a large number of possible calculation methods,[12] is not an experimental observable. Therefore, validation of calculated atomic charges against experimental benchmarks is very challenging.[13,14] Consequently, there is no agreed optimum method of calculating atomic charges, leading to worries over any conclusions drawn from atomic charges on electrostatic interactions in ILs.

Element-specific core-level X-ray photoelectron spectroscopy (XPS) binding energies, E_B(core), are experimentally observable local electronic structure descriptors that can be measured for all core-levels (bar H and He). XPS of ILs for many elements has been published (*e.g.* C, N, O, F, P, S, Cl, metals), with multiple independent research groups providing consistent and reproducible experimental E_B(core), E_B(core,exp).[13–24] For certain elements in different bonding environments, a large range of E_B(core,exp) values for both cations and anions are observed,

---

[a] *Department of Chemistry, University of Reading, Reading, UK. E-mail: k.r.j.lovelock@reading.ac.uk*

[b] *School of Engineering and Materials Science, Queen Mary University of London, London, UK*

e.g. $E_B(N_{cation}\ 1s)$ ~ 402 eV for $[C_8C_1Im]^+$ and $E_B(N_{anion}\ 1s)$ = 397.8 eV for $[SCN]^-$;[14] ~3 eV represents a very large E_B(core,exp) difference for core-level XPS. Furthermore, we have successfully established linear correlations between $E_B(N_{cation}$ 1s,exp) and anion basicity/electron donor ability, such as hydrogen bond acceptor values and electron donor numbers,[25] demonstrating that E_B(core,exp) captures key features of cation–anion interactions of ILs and highlighting the promise of E_B(core,exp) for probing non-covalent interactions in ILs.

To avoid problems with atomic charges we use the electrostatic potential at a nucleus, V_n, to characterise the local electronic structure. What we refer to here as V_n is also known in the literature with different names and acronyms: the electrostatic potential at nuclei (EPN);[26,27] the molecular electrostatic potential at the atomic sites (MEP@AS);[28] the molecular electrostatic potential (MESP) at a nucleus/reaction centre specific to an atom;[29] the site electrostatic potential.[25,30] V_n has great promise as a local electronic structure descriptor for ILs as it is, unlike atomic charges, a rigorously defined quantum mechanical quantity that reflects the potential due to all electrons and other nuclei. Furthermore, linear correlations have been found between V_n and a wide range of (mainly) non-covalent interaction strength data,[29,31,32] although not for ILs as of yet. For two ions/molecules, the atoms with large V_n on one ion/molecule will non-covalently interact strongly with atoms with small V_n on the other ion/molecule, potentially giving favourable non-covalent/non-bonded interactions.[33,34]

To establish links between E_B(core) and V_n, it is first essential to establish whether initial-state contributions (*i.e.* ground-state) or final-state contributions (*i.e.* effects after the core-hole is created in the XPS photoemission process) dominate differences in E_B(core), denoted here as ΔE_B(core), for different chemical environments, *e.g.* $E_B(N_{cation}\ 1s)$ for $[C_8C_1Im]^+$ *versus* $E_B(N_{anion}\ 1s)$ for $[SCN]^-$. There is growing evidence for ILs that initial-state effects dominate ΔE_B(core).[24,25,30,35] Results for three $[A][C_8C_1Im]$ ILs show that experimental cation E_B(C 1s,exp) and E_B(N 1s,exp) linearly correlate with calculated cation C 1s and N 1s core-level (Kohn–Sham) energies, E_B(C 1s,calc) and E_B(N 1s,calc); the anion electronic structure was not checked for correlations in that study.[25]

The charge potential model for XPS provides a simple physical explanation for ΔE_B(core) based on the ground-state electrostatic potentials at the nuclei caused by the surrounding charges.[36,37] The standard approach in XPS analysis is to use atomic charges as representatives of this potential to compare to E_B(core,exp),[37–39] but this approach is unsatisfactory given the already explained challenges with atomic charges. This approach of comparing E_B(core,exp) to V_n does not seem to have been used in the literature beyond our own recent work[25,30] and one other study of simple carbonyl molecules.[40] For three $[A][C_8C_1Im]$ ILs we showed that cation $E_B(C_{cation}$ 1s,exp) and $E_B(N_{cation}$ 1s,exp) linearly correlate with calculated V_C and V_N respectively.[25] However, comparisons of E_B(core,exp) and V_n for anions *versus* anions and, most importantly, cations *versus* anions (due to the very different formal charges of the ions), are still to be made, leaving unanswered the key question of whether E_B(core,exp) can be used to predict V_n for ILs.

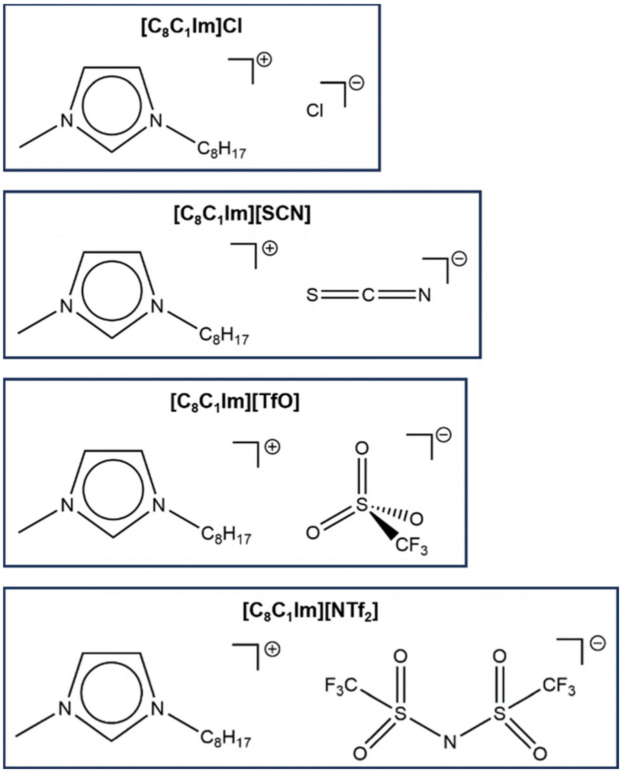

Fig. 1 Structures of the four ILs studied here. From top to bottom: 1-octyl-3-methylimidazolium chloride ($[C_8C_1Im]Cl$), 1-octyl-3-methylimidazolium thiocyanate ($[C_8C_1Im][SCN]$), 1-octyl-3-methylimidazolium trifluoromethanesulfonate ($[C_8C_1Im][TfO]$) and 1-octyl-3-methylimidazolium (bis[(trifluoromethane)sulfonyl]imide) ($[C_8C_1Im][NTf_2]$).

In this work, we compare values of atomic (*i.e.* local) electronic structure descriptors (calculated E_B(core), E_B(core,calc), and V_n) from AIMD of four $[A][C_8C_1Im]$ ILs (where $[A]^-$ = Cl^-, $[SCN]^-$, $[TfO]^-$ and $[NTf_2]^-$, Fig. 1) to E_B(core,exp) from experimental core-level XPS. All ions chosen are important in IL research and applications, where the dialkylimidazolium cation $[C_nC_1Im]^+$ is the most widely-investigated cation in ILs. The anions chosen span a wide range of anion interaction strengths,[25] and $[NTf_2]^-$ and $[TfO]^-$ are of great interest in the battery community.[41,42] Moreover, the anions chosen represent a wide range of different bonding environments (Fig. 1). For anions *versus* anions, $[SCN]^-$ has very different $E_B(N_{anion}$ 1s,exp) and $E_B(S_{anion}$ 2p,exp) to $[NTf_2]^-$ and $[TfO]^-$. For cations *versus* anions, $[NTf_2]^-$ and $[TfO]^-$ have very different E_B(C 1s,exp) to $[C_8C_1Im]^+$, and $[NTf_2]^-$ and $[SCN]^-$ have very different E_B(N 1s,exp) to $[C_8C_1Im]^+$. For cations *versus* cations, we extend our previous study of the influence of the anion on the cation[25] by including $[TfO]^-$ in our comparisons of $[C_8C_1Im]^+$ $E_B(N_{cation}\ 1s)$, $E_B(C_{hetero}\ 1s)$ and $E_B(C^2\ 1s)$.

2. Methods

2.1. Experimental: IL drop XPS

For four ILs ($[C_8C_1Im][NTf_2]$, $[C_8C_1Im][SCN]$, $[C_8C_1Im][TfO]$ and $[C_8C_1Im]Cl$, Fig. 1 and SI, Table S1), core-level XP spectra were already published, with high sample purity demonstrated.[43] E_B(core,exp) values for this XPS data are published together for the first time here (SI, Tables S6–S10), and were previously published across ref. 13, 14, 24, 25.

2.2. *Ab initio* molecular dynamics

AIMD calculations were performed for four ILs: $[C_8C_1Im][NTf_2]$, $[C_8C_1Im][SCN]$, $[C_8C_1Im][TfO]$ and $[C_8C_1Im]Cl$. A 32-ion-pair model for each IL was simulated with the Quickstep code in CP2K, using the Gaussian and Plane Wave (GPW) method with the direct inversion in iterative subspace (DIIS) technique. This same method was used previously for $[C_8C_1Im][NTf_2]$, $[C_8C_1Im][SCN]$ and $[C_8C_1Im]Cl$.[25] The density and temperature used for $[C_8C_1Im][TfO]$ was 1.17 g cm^{-3} and 398 K respectively. The increased simulation temperature was used to reduce viscosity in the system and allow for faster equilibration, reducing computational cost while still avoiding thermal decomposition. After pre-equilibration of the model with 32 ion pairs, CP2K was run for 30 ps at a timestep of 1 fs in the canonical (NVT) ensemble, controlled by a Nosé thermostat. The Perdew–Burke–Ernzerhof (PBE) functional[44] was used with Grimme's D2 corrections[45,46] to account for dispersion interactions.

2.3. Core-level binding energy and electrostatic potential at a nucleus (V_n) calculation

Calculations of the E_B(core,calc) and V_n were performed with single-point calculations using plane-wave-based density functional theory (DFT) as implemented in the Vienna ab initio simulation package (VASP).[47] The PBE exchange correlation functional, and the projector-augmented wave (PAW) potentials were employed. For the plane wave basis set expansion, the kinetic energy cutoff was set to 400 eV for all ILs. Three configurations of average potential energy were taken from the last 10 ps of the CP2K simulation for each IL to obtain values for E_B and V_n – in total 96 ion pairs (3 × 32 ion pairs) per IL. All E_B(core,calc) were calculated using the initial-state approximation, which in VASP involves re-calculating the core-level Kohn–Sham energies in the presence of the effective valence potential, assuming no relaxation of the valence electrons upon the core-hole creation.

The V_n values are derived for nucleus A at position R_A from eqn (1).[29]

$$V_n(\mathbf{R}_A) = \sum_{B \neq A} \frac{Z_B}{|\mathbf{R}_B - \mathbf{R}_A|} - \int \frac{\rho(\mathbf{r})d^3\mathbf{r}}{|\mathbf{R}_A - \mathbf{r}|} \tag{1}$$

where Z_B is the charge on nucleus B at a position R_B and $\rho(\mathbf{r})$ is the electron density at the point $\mathbf{r}$.

Average values of E_B(core,calc) and V_n were produced, labelled as E_B(core,calc,ave) and V_n(ave) respectively.

2.4. Producing calculated XP spectra and calculated V_n "spectra"

To produce calculated XP spectra for orbitals that have spin–orbit coupling (S 2p), each E_B(S 2p,calc) value was adjusted to produce E_B(S $2p_{3/2}$,calc) and E_B(S $2p_{1/2}$,calc) of the appropriate relative intensity (using E_B and area factors given in Table S2). Once E_B(S $2p_{3/2}$,calc) and E_B(S $2p_{1/2}$,calc) were obtained, a Gaussian–Lorentzian Product (GLP) function was applied to each E_B(S $2p_{3/2}$,calc) and E_B(S $2p_{1/2}$,calc) data point for each core-state using eqn (2) and then summed to produce calculated XP spectra. The mixing parameter, m, and function width, F, were set to the values given in Table S2. V_n "spectra" were produced in the same way as XP spectra (eqn (3) and Table S3).

To produce calculated XP spectra for orbitals that do not have spin–orbit coupling (N 1s, C 1s), a Gaussian–Lorentzian Product (GLP) function was applied to each E_B(core,calc) data point for each valence-state using eqn (2) and then summed to produce calculated XP spectra. Here E_B represents the precise calculated binding energy for each core-level and x represents the continuous axis of binding energies at which the intensities are calculated. The mixing parameter, m (different to the gradient m introduced in the results section for correlation plots), and function width, F, were set to the values given in Table S2. V_n "spectra" were produced in the same way as XP spectra, *i.e.* x is V_n at which the intensity is calculated (eqn (3) and Table S3).

$$\mathrm{GLP}(x; F, E_B, m) = \frac{\exp\left[-4\ln 2(1-m)\dfrac{(x-E_B)^2}{F^2}\right]}{\left[1 + 4m\dfrac{(x-E_B)^2}{F^2}\right]} \tag{2}$$

$$\mathrm{GLP}(x; F, V_n, m) = \frac{\exp\left[-4\ln 2(1-m)\dfrac{(x-V_n)^2}{F^2}\right]}{\left[1 + 4m\dfrac{(x-V_n)^2}{F^2}\right]} \tag{3}$$

3. Results and discussion

3.1. Initial-state effects dominate ΔE_B(core)

For datasets with contributions from both cations and anions, there are excellent linear correlations between E_B(core,exp) and E_B(core,calc,ave) (Fig. 2a and b). Four different $[A][C_8C_1Im]$ ILs contributed data points from $[C_8C_1Im]^+$ to E_B(core,calc,ave); $[A]^-$ = $[NTf_2]^-$, $[SCN]^-$, $[TfO]^-$ and Cl^-. The coefficient of determination, R^2, is very close to 1 for both N 1s and C 1s (Fig. 2a and b respectively), indicating excellent linear correlation; for example, for N 1s data $R^2 = 1.00$ (Fig. 2a). Gradients, m, are very close to 1, indicating nearly identical relative values; for example, for N 1s data $m = 0.97$ (Fig. 2a).

Qualitative matches between experimental and calculated XP spectra for N 1s and C 1s (Fig. 3a–d, respectively) are observed, with N 1s XP spectra for both cations and anions giving particularly good qualitative matches. This captures both (a) the effect of the anion on the $[C_8C_1Im]^+$ cation and (b) cations *versus* anions, demonstrating clearly that initial-state effects dominate ΔE_B(N 1s).

Comparisons of experimental and calculated XP spectra for anions *versus* anions are striking. There are excellent linear

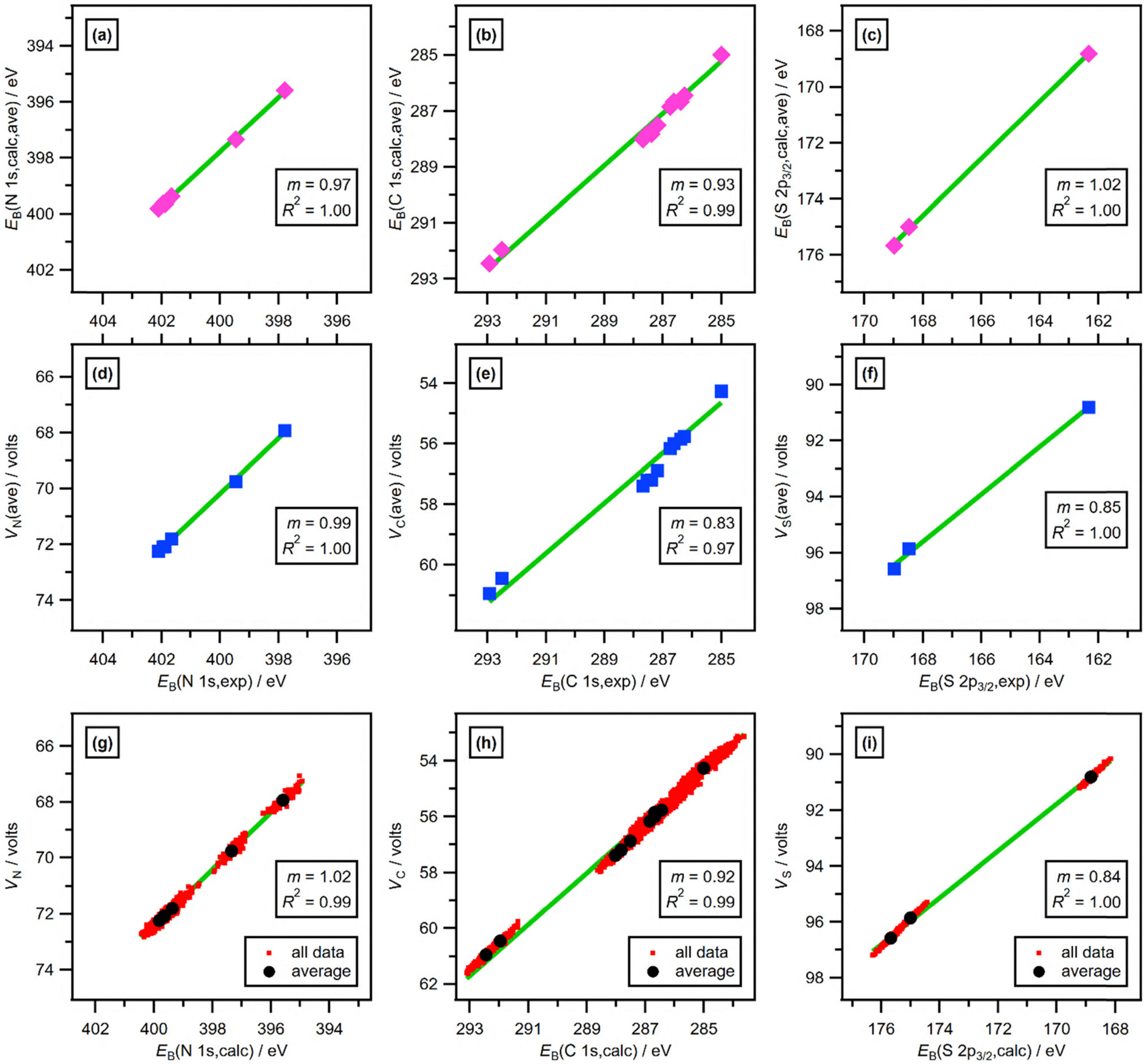

Fig. 2 E_B(core,calc,ave) plotted against E_B(core,exp) for [C_8C_1Im]Cl, [C_8C_1Im][SCN], [C_8C_1Im][TfO] and [C_8C_1Im][NTf_2]: (a) N 1s (data for both cations and anions), (b) C 1s (data for both cations and anions), (c) S $2p_{3/2}$ (data for anions). V_n(ave) plotted against E_B(core,exp) for [C_8C_1Im]Cl, [C_8C_1Im][SCN], [C_8C_1Im][TfO] and [C_8C_1Im][NTf_2]: (d) N 1s (data for both cations and anions), (e) C 1s (data for both cations and anions), (f) S $2p_{3/2}$ (data for anions). V_n (all individual data points and average) plotted against E_B(core,calc) for [C_8C_1Im]Cl, [C_8C_1Im][SCN], [C_8C_1Im][TfO] and [C_8C_1Im][NTf_2]: (g) N 1s (data for both cations and anions), (h) C 1s (data for both cations and anions), (i) S $2p_{3/2}$ (data for anions). R^2 = coefficient of determination and m = gradient. Full equations for the correlations are given in SI, Table S12.

correlations between E_B(S $2p_{3/2}$,exp) and E_B(S $2p_{3/2}$,calc,ave) from AIMD on 32 ion pairs of two different anions in [A][C_8C_1Im] ILs, where $[A]^-$ = $[NTf_2]^-$ and $[SCN]^-$, as demonstrated by R^2 very close to 1 (Fig. 2c).

Qualitative matches between experimental and calculated XP spectra for S 2p (Fig. 4c and f) are excellent, supporting the findings, from the linear correlations, that initial-state effects dominate ΔE_B(core). Furthermore, there are noteworthy qualitative matches between experimental and calculated XP spectra for N_{anion} 1s (Fig. 3a and c), C_{anion} 1s (Fig. 3b and d), F_{anion} 1s (Fig. 4a and d) and O_{anion} 1s (Fig. 4b and e).

The qualitative matches of C 1s XP spectra are slightly less perfect than for N 1s. Firstly, for anionic CF_3 1s *versus* cationic C_{alkyl} 1s, ΔE_B(core,exp) is slightly larger than ΔE_B(core,calc) (~0.5 eV, Fig. 3b and d). Secondly, for cationic C^2 1s *versus* cationic C_{hetero} 1s *versus* cationic C_{alkyl} 1s, ΔE_B(core,exp) is slightly smaller than the calculated ΔE_B(core,calc) (~0.5 eV). These relatively small ΔE_B(C 1s) mismatches could reflect small differences in final-state effects for the different types of carbon or DFT-related differences (which might be resolved by a more expensive method that is not currently feasible for such large IL simulation boxes); they are not due to cation *versus* anion

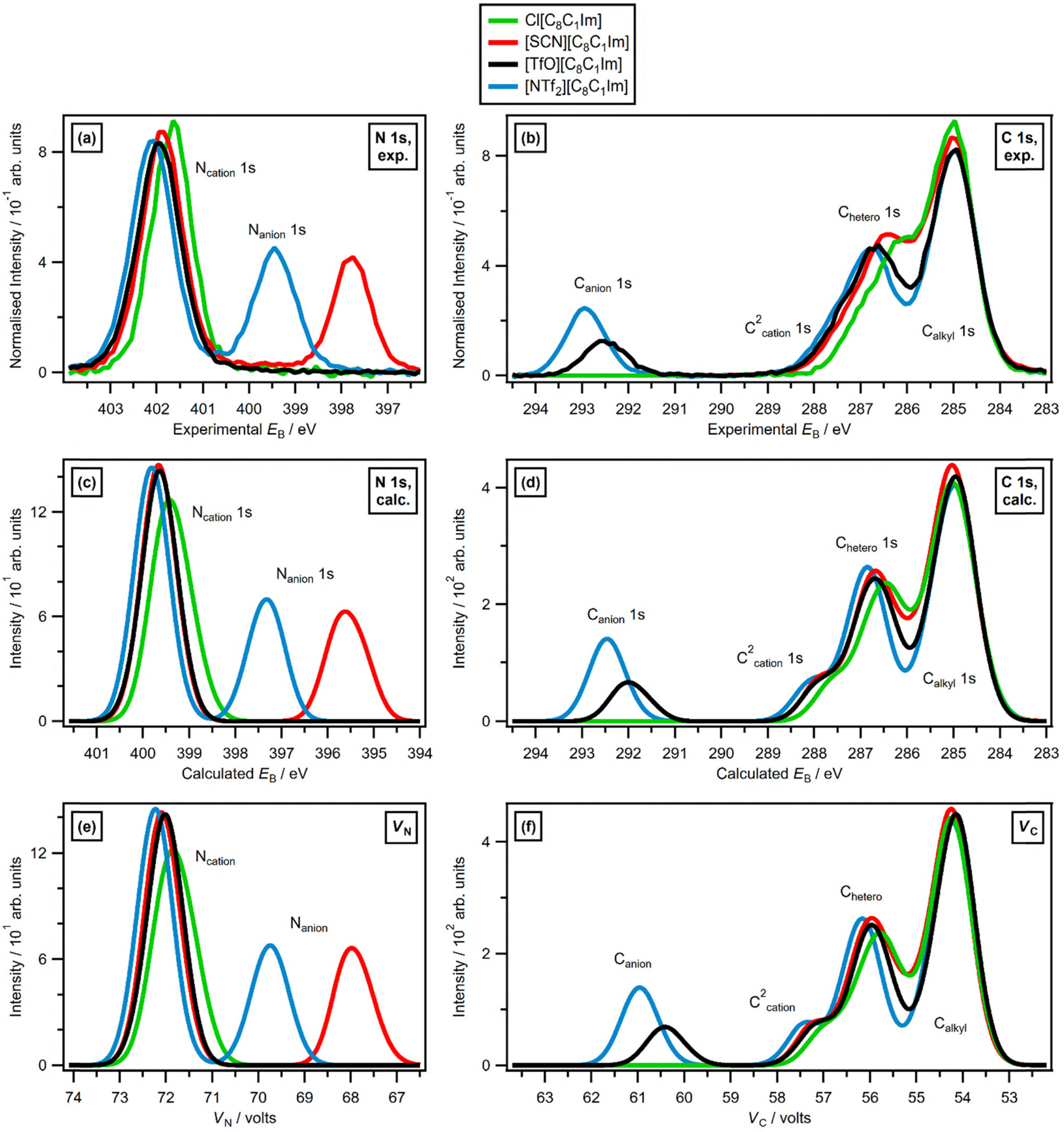

Fig. 3 Experimental and calculated data for [A][C_8C_1Im] where $[A]^-$ = Cl^-, $[SCN]^-$, $[TfO]^-$ and $[NTf_2]^-$. Experimental core-level XPS: (a) N 1s, (b) C 1s. Calculated core-level XPS: (c) N 1s, (d) C 1s. Electrostatic potential at nucleus: (e) V_N, (f) V_C. Experimental XP spectra are area normalised and charge referenced using methods given in SI, Section S4. Calculated XP spectra and V_n data are charge referenced using methods given in SI, Section S4.

effects, as there are mismatches for both cation *versus* cation and anion *versus* cation.

Initial-state effects dominate ΔE_B(core) for the same element, as demonstrated by both the excellent linear correlations between E_B(core,exp) and E_B(core,calc) and by the qualitative matches between experimental and calculated XP spectra. Final-state effects are approximately constant for all atoms of the same element. This observation demonstrates that final-state effects are not linked to the ionic nature of ILs where cations and anions might be expected to have different final-state effects due to the formal charges of the ions.

Our findings show that initial-state effects dominate ΔE_B(core). This finding agrees with previous results for 17 gas-phase nitrogen-containing molecules, and also with our

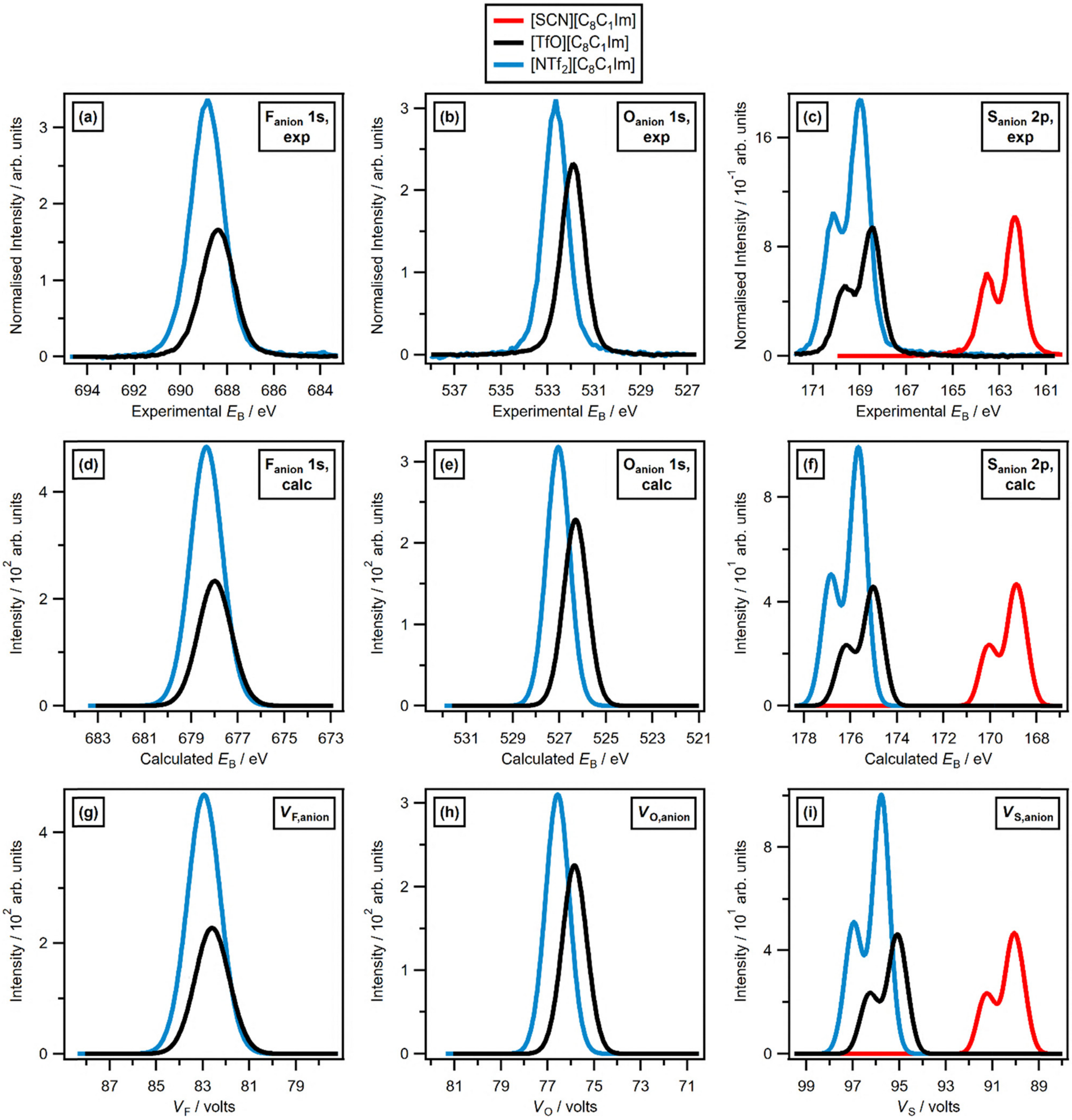

Fig. 4 Experimental and calculated data for [A][C_8C_1Im] where $[A]^-$ = $[SCN]^-$, $[TfO]^-$ and $[NTf_2]^-$. Experimental core-level XPS: (a) F 1s, (b) O 1s, (c) S 2p. Calculated core-level XPS: (d) F 1s, (e) O 1s, (f) S 2p. Electrostatic potential at nucleus: (g) V_F, (h) V_O, (i) V_S. Experimental XP spectra are area normalised and charge referenced using methods given in SI, Section S4. Calculated XP spectra and V_n data are charge referenced using methods given in SI, Section S4.

recent comparisons of E_B(core) for ILs (where E_B(core,calc) came from small-scale DFT and not AIMD, hence cation–anion interactions were not included).[24,48]

Final-state effects are either minimal or are constant across all atoms for the same element in the four different ILs. Chemical intuition could lead one to expect final-state effects to be different for atoms in the cations and anions given the significant difference in formal charges, but that is not the case. Therefore, the formal charge of the ion does not have a strong influence on the magnitude of the final-state effect contributions.

3.2. ΔE_B(core) captures ΔV_n

ΔE_B(core,exp) describes ΔV_n(ave) very well and ΔE_B(core,calc) describes ΔV_n very well, including comparisons of cations *versus* anions, anions *versus* anions and cations *versus* cations. Larger E_B(core) gives larger V_n and smaller E_B(core) gives smaller V_n (Fig. 2d–i).

There are excellent linear correlations between E_B(N 1s,exp) and V_N(ave) (Fig. 2d), E_B(C 1s,exp) and V_C(ave) (Fig. 2e), and E_B(S $2p_{3/2}$,exp) and V_S(ave) (Fig. 2f); there is insufficient data for fluorine, oxygen and chlorine to obtain linear correlations (SI, Fig. S1). There are also excellent linear correlations between E_B(N 1s,calc) and V_N (Fig. 2g), E_B(C 1s,calc) and V_C (Fig. 2h), E_B(S $2p_{3/2}$,calc) and V_S (Fig. 2i), E_B(F 1s,calc) and V_F (SI, Fig. S1e), E_B(O 1s,calc) and V_O (SI, Fig. S1f), E_B(Cl $2p_{3/2}$,calc) and V_{Cl} (SI, Fig. S1g).

Both E_B(core,exp) and E_B(core,calc) capture very well the order of the changes in V_n. R^2 are all ≥ 0.97, so very near 1, for E_B(core,exp) *versus* V_n(ave) (Fig. 2d–f) and E_B(core,calc) *versus* V_n (Fig. 2g–i and SI, Fig. S1e–g). There are superb qualitative visual matches between experimental XP spectra, calculated XP spectra and V_n "spectra": nitrogen (Fig. 3a, c and e), carbon (Fig. 3b, d and f), sulfur (Fig. 4c, f and i), fluorine (Fig. 4a, d and g), oxygen (Fig. 4b, e and h). For example, for comparisons of sulfur, the orders of E_B(core,exp), E_B(core,calc,ave) and V_n(ave) are always $[NTf_2]^- > [TfO]^- > [SCN]^-$ (Fig. 4c, f and i).

The gradients, *m*, for the linear correlations for E_B(N 1s) *versus* V_N are both almost 1.00 (Fig. 2d and g), and the qualitative matches of N 1s XP spectra and V_N "spectra" are almost perfect (Fig. 3a, c and e). For N_{cation} from $[C_8C_1Im][NTf_2]$ *versus* N_{anion} from $[C_8C_1Im][SCN]$, ΔE_B(core,exp) = 4.31 eV, ΔE_B(core,calc,ave) = 4.23 eV, and ΔV_N(ave) = 4.31 eV (SI, Table S8), *i.e.* the same within experimental uncertainty. These observations confirm that E_B(N 1s) represent measures of V_N at the atoms in question.

Both ΔE_B(core,exp) and ΔE_B(core,calc) do not always capture the exact magnitude of ΔV_n. The gradients, *m*, for the linear correlations for E_B(S $2p_{3/2}$) *versus* V_S are both $\sim$0.85 (Fig. 2f and i), and the qualitative matches of S 2p XP spectra and V_S "spectra" show small but significant differences (Fig. 4c, f and i). For example, S 2p for $[SCN]^-$ *versus* $[TfO]^-$ gives ΔE_B(core,exp) = 6.14 eV, ΔE_B(core,calc,ave) = 6.18 eV and ΔV_n(ave) = 5.05 eV (SI, Table S10), *i.e.* larger differences than experimental uncertainty. Furthermore, the gradients, *m*, for the linear correlations for E_B(C1s) *versus* V_C are 0.83 and 0.92 (Fig. 2e and h), and the qualitative visual matches of C 1s XP spectra and V_C "spectra" show small but significant differences (Fig. 3b, d and f).

These observations highlight that both E_B(core,exp) and E_B(core,calc) have small contributions from sources other than V_n. The mismatches for sulfur are for comparisons of anion *versus* anion, showing that the mismatches are not primarily caused by differences in formal charges on cations and anions. Therefore, these small contributions are most likely from exchange–correlation contributions to E_B(core) that of course do not influence V_n, as also suggested for gas-phase calculations of 17 nitrogen-containing molecules.[48]

Overall, E_B(core) can be used as chemically interpretable experimental descriptors that represent V_n, given the matches ranging from good to excellent (*e.g.* E_B(core) *versus* V_n is near-perfect for $[TfO]^-$). With strong links between E_B(core) *versus* V_n and E_B(core) *versus* Kamlet–Taft β values *etc.*, we show that the interactions are strongly driven by electrostatics, and so calculated V_n values are a valid method of measuring anion interaction strength. Given the large range of E_B(core) considered for anions for multiple elements, we expect that the correlations presented here for four ILs will hold for other ILs with different anions. Whilst one dialkylimidazolium-based cation is studied here, the findings will very likely hold for other aprotic aromatic and non-aromatic organic cations, *e.g.* tetraalkylammonium, tetraalkylphosphonium, alkylpyridinium, dialkylpyrrolidinium, as experimental XPS shows the same influence of anions on these cations as dialkylimidazolium.[25,49–51] The findings might hold for both protic cations (*e.g.* protic ammonium cations for lignocellulosic biomass fractionation[52]) and metal cations (*e.g.* Li^+ for battery electrolyte research[2]), but further studies are required for these cations.

Murray and Politzer noted that V_n varies very little for different chemical environments of the same element.[53] The same is true for E_B(core) for the same core-level of the same element, *e.g.* for E_B(C 1s,exp) the range of values is 7.93 eV (SI, Table S9), which is $\sim$3% of the average E_B(C 1s,exp) value of $\sim$287 eV. However, those small differences in V_n and also in E_B(core), or "minor perturbations" as Politzer calls them,[53] contain huge amounts of information on changes in the electron density near the atom in question and therefore in bonding. In other words, despite such small percentage changes in E_B(core) and V_n values, E_B(core) and V_n still represent very useful chemical descriptors.

The link between E_B(core) and V_n matches to the initial-state effect driven rationalisations for ΔE_B(core) that date back to Siegbahn and co-workers in the 1960s,[54] where for sulfur-containing compounds more positive atomic charge for sulfur atoms was correlated to larger E_B(S 2p,exp) and more negative atomic charge for sulfur gave smaller E_B(S 2p,exp). The most common description of the charge potential model in XPS is to use atomic charges of neighbouring atoms to calculate E_B(core) but here we propose using V_n (*i.e.* surrounding electrons and nuclei) instead. Therefore, a refinement of the charge potential model for XPS[36,37] can be proposed; instead of using atomic charges to explain and possibly predict E_B(core), V_n can be used instead.

E_B(core,calc,ave) for each type of atom in an AIMD calculation can give the V_n(ave) for each type of that atom, demonstrating a major advantage of the calculations over experimental XPS. One limitation of using E_B(core,exp) as experimental descriptors of V_n is that not all covalently non-equivalent atoms can be distinguished. For example, the terminal CH_3 carbon on the butyl chain in $[C_4C_1Im]^+$ is indistinguishable in XPS from the CH_2 carbon bonded to this CH_3 group (unlike in NMR spectroscopy, where these two carbons can be distinguished). Furthermore, the experimental carbon contribution from the $[SCN]^-$ anion cannot be separated from the experimental carbon contribution from the $[C_8C_1Im]^+$ cation,[30] but such separations are possible for the calculated data.

4. Summary and conclusions

Core-level binding energies, E_B(core), are presented here as an atomic (*i.e.* local) electrostatic interaction strength descriptor for ILs, capturing differences in electrostatic potentials at the nuclei, V_n. We believe E_B(core) will prove useful for rationalising IL properties, especially since E_B(core) is readily interpretable in terms of V_n. Effective measurements of ΔV_n are achievable using experimental core-level XPS of ILs. Therefore, E_B(core) from core-level XPS capture the potential for the atom/group of atoms in question, relative to other atoms of the same element in the same ion or different ions.

The already extensive literature IL ΔE_B(core,exp) dataset, in combination with the significant new physical insights given here, opens many avenues for future work, including: (1) the comparison of E_B(core) *versus* V_n for protic organic cations and metal cations; (2) the prediction of ΔV_n without the need for expensive and technically-demanding calculations; (3) the re-evaluation of anion ΔE_B(core,exp) in terms of electrostatic interaction strengths, especially as in our previous publication the focus was on cation ΔE_B(core,exp);[25] and (4) a more accurate grouping of types of atoms in ILs, as currently groupings are made based on qualitative assessments of electronic structure (*e.g.* charged groups, hydrocarbons, fluorous[8]) and not on experimental electronic structure data.

An interesting question is whether the excellent matches between E_B(core) and V_n would also work for E_B(core) of ions or even neutral molecules solvated in (neutral) molecular solvents rather than solvated in ILs. E_B(core,exp) for ions solvated in (neutral) molecular solvents are not available yet for the ions studied here or indeed many other ions, although E_B(core,exp) can be measured using liquid-jet XPS apparatus.[55] Furthermore, can E_B(core) and V_n be interpreted at surfaces and interfaces to link to processes such as IL adsorption and IL electrochemistry?

Measuring new ΔE_B(core,exp) values beyond those already available in the extensive but certainly incomplete literature will require expensive IL synthesis and XPS measurement. Another option is aiming to achieve a method that is cheap and technically undemanding (unlike our method presented here). Modern machine learning methods offer fantastic possibilities in this area, both for predicting IL structures using machine learning potentials[56] and using structure descriptors to predict electronic structure properties.[57] A combination of such methods would potentially allow rapid prediction of accurate E_B(core,calc) and V_n, allowing screening of large numbers of ILs.

Conflicts of interest

There are no conflicts to declare.

Data availability

Data for this article, including log files for all new calculated structures, are available at University of Reading Research Data Archive, DOI: **https://doi.org/10.17864/1947.001453**.

Analysed data supporting this article have been included as part of the supplementary information (SI). Supplementary information is available. See DOI: **https://doi.org/10.1039/d5cp02411k**.

Acknowledgements

We are grateful to the UK Materials and Molecular Modelling Hub for access to the Young supercomputer facility, which is partially funded by the EPSRC (EP/T022213/1). This work also used the ARCHER2 UK National Supercomputing Service, *via* the Materials Chemistry Consortium, which is also funded by EPRSC (EP/R029431/1). We acknowledge support from a Royal Society University Research Fellowship (URF\R\150353, URF\R\211005, RGF\EA\180089, RGF\R1\180053, RF\ERE\210061 and RF\ERE\231015). Dr Richard Matthews is thanked for helpful discussions.

References

1 D. R. MacFarlane, N. Tachikawa, M. Forsyth, J. M. Pringle, P. C. Howlett, G. D. Elliott, J. H. Davis, M. Watanabe, P. Simon and C. A. Angell, *Energy Environ. Sci.*, 2014, **7**, 232–250.
2 D. R. MacFarlane, M. Forsyth, P. C. Howlett, M. Kar, S. Passerini, J. M. Pringle, H. Ohno, M. Watanabe, F. Yan, W. J. Zheng, S. G. Zhang and J. Zhang, *Nat. Rev. Mater.*, 2016, **1**, 15005.
3 T. Zhou, C. M. Gui, L. G. Sun, Y. X. Hu, H. Lyu, Z. H. Wang, Z. Song and G. Q. Yu, *Chem. Rev.*, 2023, **123**, 12170–12253.
4 Z. Y. Zhao, H. Li and X. Gao, *Chem. Rev.*, 2023, **124**, 2651–2698.
5 J. L. Shamshina and R. D. Rogers, *Chem. Rev.*, 2023, **123**, 11894–11953.
6 X. Q. Li, K. Chen, R. L. Guo and Z. Wei, *Chem. Rev.*, 2023, **123**, 10432–10467.
7 G. X. Li, K. Chen, Z. G. Lei and Z. Wei, *Chem. Rev.*, 2023, **123**, 10258–10301.
8 R. Hayes, G. G. Warr and R. Atkin, *Chem. Rev.*, 2015, **115**, 6357–6426.
9 C. Merlet, B. Rotenberg, P. A. Madden, P. L. Taberna, P. Simon, Y. Gogotsi and M. Salanne, *Nat. Mater.*, 2012, **11**, 306–310.
10 Y. Ge, Q. Zhu, X. P. Wang and J. Ma, *Ind. Chem. Mater.*, 2025, **3**, 383–411.
11 S. Koutsoukos, F. Philippi, F. Malaret and T. Welton, *Chem. Sci.*, 2021, **12**, 6820–6843.
12 C. J. Cramer, *Essentials of Computational Chemistry: Theories and Methods*, Wiley, John Wiley & Sons, Chichester, 2002.
13 R. M. Fogarty, R. Rowe, R. P. Matthews, M. T. Clough, C. R. Ashworth, A. Brandt, P. J. Corbett, R. G. Palgrave, E. F. Smith, R. A. Bourne, T. W. Chamberlain, P. B. J. Thompson, P. A. Hunt and K. R. J. Lovelock, *Faraday Discuss.*, 2018, **206**, 183–201.
14 R. M. Fogarty, R. P. Matthews, C. R. Ashworth, A. Brandt-Talbot, R. G. Palgrave, R. A. Bourne, T. V. Hoogerstraete, P. A. Hunt and K. R. J. Lovelock, *J. Chem. Phys.*, 2018, **148**, 193817.

15 K. R. J. Lovelock, I. J. Villar-Garcia, F. Maier, H. P. Steinrück and P. Licence, *Chem. Rev.*, 2010, **110**, 5158–5190.

16 T. Cremer, C. Kolbeck, K. R. J. Lovelock, N. Paape, R. Wölfel, P. S. Schulz, P. Wasserscheid, H. Weber, J. Thar, B. Kirchner, F. Maier and H. P. Steinrück, *Chem. – Eur. J.*, 2010, **16**, 9018–9033.

17 I. J. Villar-Garcia, E. F. Smith, A. W. Taylor, F. L. Qiu, K. R. J. Lovelock, R. G. Jones and P. Licence, *Phys. Chem. Chem. Phys.*, 2011, **13**, 2797–2808.

18 B. B. Hurisso, K. R. J. Lovelock and P. Licence, *Phys. Chem. Chem. Phys.*, 2011, **13**, 17737–17748.

19 M. Reinmöller, A. Ulbrich, T. Ikari, J. Preiss, O. Höfft, F. Endres, S. Krischok and W. J. D. Beenken, *Phys. Chem. Chem. Phys.*, 2011, **13**, 19526–19533.

20 A. W. Taylor, S. Men, C. J. Clarke and P. Licence, *RSC Adv.*, 2013, **3**, 9436–9445.

21 J. M. Seymour, E. Gousseva, F. K. Towers Tompkins, L. G. Parker, N. O. Alblewi, C. J. Clarke, S. Hayama, R. G. Palgrave, R. A. Bennett, R. P. Matthews and K. R. J. Lovelock, *Faraday Discuss.*, 2024, **253**, 251–272.

22 R. M. Fogarty, R. P. Matthews, P. A. Hunt and K. R. J. Lovelock, *Phys. Chem. Chem. Phys.*, 2025, **27**, 9068–9075.

23 J. M. Seymour, E. Gousseva, L. G. Parker, F. K. T. Tompkins, R. M. Fogarty, L. Frankemoelle, R. Rowe, C. J. Clarke, D. A. Duncan, R. G. Palgrave, R. A. Bennett, P. A. Hunt and K. R. J. Lovelock, *J. Phys. Chem. Lett.*, 2025, **16**, 2831–2836.

24 F. K. Towers Tompkins, L. G. Parker, R. M. Fogarty, J. M. Seymour, R. Rowe, R. G. Palgrave, R. P. Matthews, R. A. Bennett, P. A. Hunt and K. R. J. Lovelock, *Phys. Chem. Chem. Phys.*, 2025, **27**, 8803–8812.

25 E. Gousseva, F. K. Towers Tompkins, J. M. Seymour, L. G. Parker, C. J. Clarke, R. G. Palgrave, R. A. Bennett, R. Grau-Crespo and K. R. J. Lovelock, *J. Phys. Chem. B*, 2024, **128**, 5030–5043.

26 G. Koleva, B. Galabov, J. I. Wu, H. F. Schaefer and P. V. Schleyer, *J. Am. Chem. Soc.*, 2009, **131**, 14722–14727.

27 B. Galabov, V. Nikolova and S. Ilieva, *Chem. – Eur. J.*, 2013, **19**, 5149–5155.

28 M. Lesiuk and J. Zachara, *J. Chem. Phys.*, 2013, **138**, 074107.

29 C. H. Suresh and S. Anila, *Acc. Chem. Res.*, 2023, **56**, 1884–1895.

30 E. Gousseva, S. D. Midgley, J. M. Seymour, R. Seidel, R. Grau-Crespo and K. R. J. Lovelock, *J. Phys. Chem. B*, 2022, **126**, 10500–10509.

31 C. H. Suresh, G. S. Remya and P. K. Anjalikrishna, *Wiley Interdiscip. Rev.: Comput. Mol. Sci.*, 2022, **12**, e1601.

32 B. Galabov, S. Ilieva, G. Koleva, W. D. Allen, H. F. Schaefer and P. V. Schleyer, *Wiley Interdiscip. Rev.: Comput. Mol. Sci.*, 2013, **3**, 37–55.

33 P. Politzer and J. S. Murray, *ChemPhysChem*, 2020, **21**, 579–588.

34 J. S. Murray and P. Politzer, *Wiley Interdiscip. Rev.: Comput. Mol. Sci.*, 2017, **7**, e1326.

35 M. Lembinen, E. Nommiste, H. Ers, B. Docampo-Alvarez, J. Kruusma, E. Lust and V. B. Ivanistsev, *Int. J. Quantum Chem.*, 2020, **120**, e26247.

36 M. E. Schwartz, *Chem. Phys. Lett.*, 1970, **6**, 631–636.

37 *Surface Analysis: The Principal Techniques*, ed. J. C. Vickerman and I. S. Gilmore, John Wiley & Sons, Chichester, 2009.

38 *Surface Analysis by Auger and X-ray Photoelectron Spectroscopy*, ed. D. Briggs and J. T. Grant, IM Publications, Manchester, 2003.

39 K. W. Kolasinski, *Surface Science: Foundations of Catalysis and Nanoscience*, Wiley, Chichester, 4th edn, 2020.

40 R. E. Bruns, R. L. A. Haiduke and A. T. do Amaral, *J. Braz. Chem. Soc.*, 2002, **13**, 800–805.

41 Y. Yamada, J. H. Wang, S. Ko, E. Watanabe and A. Yamada, *Nat. Energy*, 2019, **4**, 269–280.

42 K. Xu, *Chem. Rev.*, 2014, **114**, 11503–11618.

43 R. M. Fogarty, R. G. Palgrave, R. A. Bourne, K. Handrup, I. J. Villar-Garcia, D. J. Payne, P. A. Hunt and K. R. J. Lovelock, *Phys. Chem. Chem. Phys.*, 2019, **21**, 18893–18910.

44 J. P. Perdew, K. Burke and M. Ernzerhof, *Phys. Rev. Lett.*, 1996, **77**, 3865–3868.

45 S. Grimme, *J. Comput. Chem.*, 2004, **25**, 1463–1473.

46 S. Grimme, *J. Comput. Chem.*, 2006, **27**, 1787–1799.

47 G. Kresse and J. Furthmüller, *Phys. Rev. B: Condens. Matter Mater. Phys.*, 1996, **54**, 11169–11186.

48 N. P. Bellafont, F. Illas and P. S. Bagus, *Phys. Chem. Chem. Phys.*, 2015, **17**, 4015–4019.

49 S. Men, D. S. Mitchell, K. R. J. Lovelock and P. Licence, *ChemPhysChem*, 2015, **16**, 2211–2218.

50 R. K. Blundell and P. Licence, *Phys. Chem. Chem. Phys.*, 2014, **16**, 15278–15288.

51 S. Men, K. R. J. Lovelock and P. Licence, *Phys. Chem. Chem. Phys.*, 2011, **13**, 15244–15255.

52 A. Brandt-Talbot, F. J. V. Gschwend, P. S. Fennell, T. M. Lammens, B. Tan, J. Weale and J. P. Hallett, *Green Chem.*, 2017, **19**, 3078–3102.

53 P. Politzer and J. S. Murray, *Mol. Phys.*, 2022, e2101563, DOI: **10.1080/00268976.2022.2101563**.

54 K. Hamrin, G. Johansson, A. Fahlman, C. Nordling, K. Siegbahn and B. Lindberg, *Chem. Phys. Lett.*, 1968, **1**, 557–559.

55 B. Winter and M. Faubel, *Chem. Rev.*, 2006, **106**, 1176–1211.

56 Z. A. H. Goodwin, M. B. Wenny, J. H. Yang, A. Cepellotti, J. X. Ding, K. Bystrom, B. R. Duschatko, A. Johansson, L. X. Sun, S. Batzner, A. Musaelian, J. A. Mason, B. Kozinsky and N. Molinari, *J. Phys. Chem. Lett.*, 2024, **15**, 7539–7547.

57 T. Zarrouk, R. Ibragimova, A. P. Bartók and M. A. Caro, *J. Am. Chem. Soc.*, 2024, **146**, 14645–14659.